Dynamics of the Garnet/Li Interface for Dendrite-Free Solid-State Batteries

Hanyu Huo[a,b], *Jianneng Liang*[a], *Ning Zhao*[c], *Xiaona Li*[a], *Xiaoting Lin*[a], *Yang Zhao*[a], *Keegan Adair*[a], *Ruying Li*[a], *Xiangxin Guo*[c *], *Xueliang Sun*[a *]

[a] Department of Mechanical and Materials Engineering, University of Western Ontario, Ontario N6A 5B9, Canada

[b] State Key Laboratory of High Performance Ceramics and Superfine Microstructure, Shanghai Institute of Ceramics, Chinese Academy of Sciences, Shanghai 200050, China

[c] College of Physics, Qingdao University, Qingdao 266071, China

[*] Corresponding authors.

Email address: xxguo@qdu.edu.cn, xsun9@uwo.ca

Experimental

Fabrication of 3D-LLZTO

Tantalum (Ta)-doped $Li_{6.4}La_3Zr_{1.4}Ta_{0.6}O_{12}$ (LLZTO) powders and dense pellets were prepared according to our previous work [1]. 1 M hydrochloric acid (HCl) was obtained by concentrated HCl (12 M) adding certain water. The LLZTO pellets were immersed in the HCl solution for 1 h. After that, the acid-treated pellets were rapidly washed by ethanol and dried by a hairdryer. Various acid-etching time was used to examine the effect on the thickness of porous structure.

Fabrication of 3D-LLZTO@ZnO

A layer of ZnO with 20 nm thickness was coated on the 3D-LLZTO surface by the atomic layer deposition (ALD) method with Gemstar-8 ALD system (Arradiance, USA). The ALD process with 150 cycles was operated in a vacuum condition and at 150 °C. Ar gas functions as the carrier gas in the whole process. Precursors diethyl zinc (DEZ) and water were used as precursors for the ALD process. The same ZnO layer was also coated on the LLZTO surface for comparison.

Materials characterizations

Crystal structures of samples were examined by X-ray diffraction (XRD, Bruker D2 Phaser), using Cu Kα radiation with 2θ in the range of 10°~80° and a step size of 0.02°. Surface and cross-section morphologies of the LLZTO pellets were investigated by scanning electron microscopy (SEM, S3400 and S4800). X-ray photoelectron spectroscopy (XPS, ESCALAB-250) were performed to characterize the composition of LLZTO pellets before and after acid-etching.

Electrochemical performance tests

Ionic conductivities of the various LLZTO samples were measured by an impedance analyzer (Novocontrol Beta High Performance Impedance Analyzer) with an AC of 10 mV from 0.1 to 7 M Hz in frequency. Thin gold layers on both surfaces of ceramic pellets were performed by magnetic sputtering as electrodes before the conductivity test. The 3D-LLZTO@ZnO pellets were sandwiched between two pieces of Li metal to construct the symmetric cells. Li metal electrodes were melted onto the two sides of the LLZTO pellets at 300 ^{o}C for 30 min in an Ar-filled glovebox before sealing in Swagelok-type cell mold. A pressure of approximately 10 N cm^{-2} was exerted on the ceramic plates via springs to keep close contact. Electrochemical impedance spectroscopy (EIS) measurements were performed in the frequency range from 1 MHz to 0.1 Hz with an amplitude of 10 mV by an Autolab instrument. Galvanostatic cycling tests were conducted using a Land battery cycler under different current densities at 25 ^{o}C. Li/LLZTO/Li and Li/LLZTO@ZnO/Li symmetric cells were also fabricated and cycled under the same procedure as a comparison. Li metal anodes with two different thickness (200 μm and 30 μm) were used for investigating the effect of Li volume change on the Li dendrite growth. The Li anode was the ~200 μm Li without any special notification. Three cells were assembled for cross-sections at different states during plating and stripping at 0.5 mA cm^{-2} (1 mAh cm^{-2}).

To fabricate “all-in-one” LFP/Li cells, the LFP, PVDF, LiTFSI, and SP with the weight ratio of LFP: LiTFSI: SP: PVDF=5: 3.5: 1: 0.5 were mixed together to fabricate cathode slurry using N-Methyl pyrrolidone (NMP) as solvent [2]. The slurry was

infiltrated into the LLZTO framework and heated at 80 °C in a vacuum oven for 12 h. The LFP loading is ~2 mg cm^{-2} and 1 C = 170 mAh g^{-1}. The ~30 μm-thick Li was infiltrated into the other side of the LLZTO porous framework. The LFP cathodes with a similar LFP loading were also coated on LLZTO and LLZTO@ZnO pellets to fabricate LFP/Li full cells for comparison. The LFP/Li cells were operated at 60 °C. The GITT was carried out with a pulse current of 0.1 C for 10 min and rest for 30 min at the 2nd cell cycle.

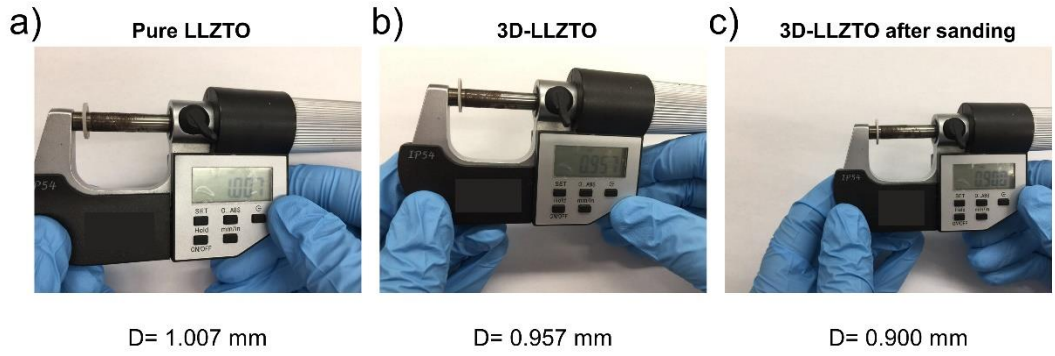

Figure S1 Thickness measurements of a) pure LLZTO, b) 3D-LLZTO by acid-etching and c) 3D-LLZTO after sanding the upper 3D layers.

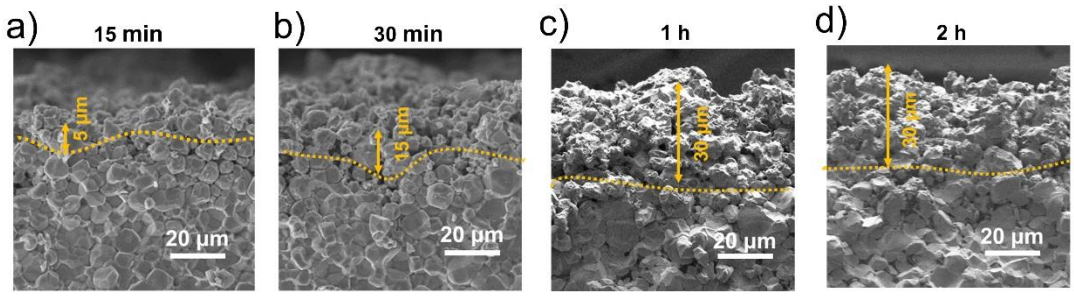

Figure S2 Cross-sectional SEM images of acid-etched 3D-LLZTO for a) 15 min, b) 30 min, c) 1 h, and d) 2 h.

As shown in Figure S2, the thickness of the porous layer increases from 5 μm to 30 μm when the time for acid etching increases from 15 min to 1 h. Further increasing the etching time cannot increase the thickness of the 3D structure, indicating a dynamic equilibrium after 1 h acid etching. In order to obtain various thicknesses and porosities of 3D LLZTO frameworks, the concentration of HCl can be changed and some surface-active agents can be added in the HCl solution, which will be studied in the future.

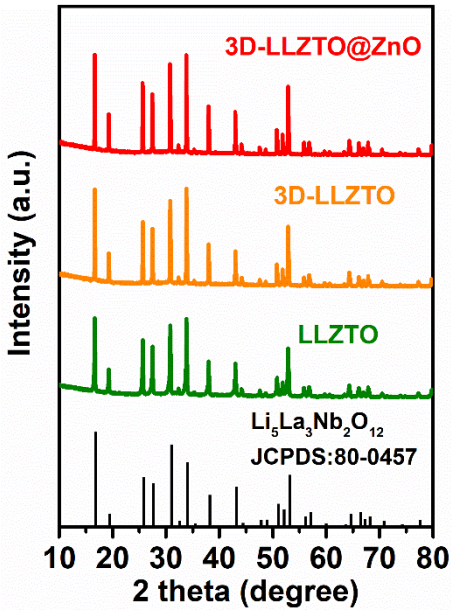

Figure S3 XRD patterns of LLZTO, 3D-LLZTO and 3D-LLZTO@ZnO.

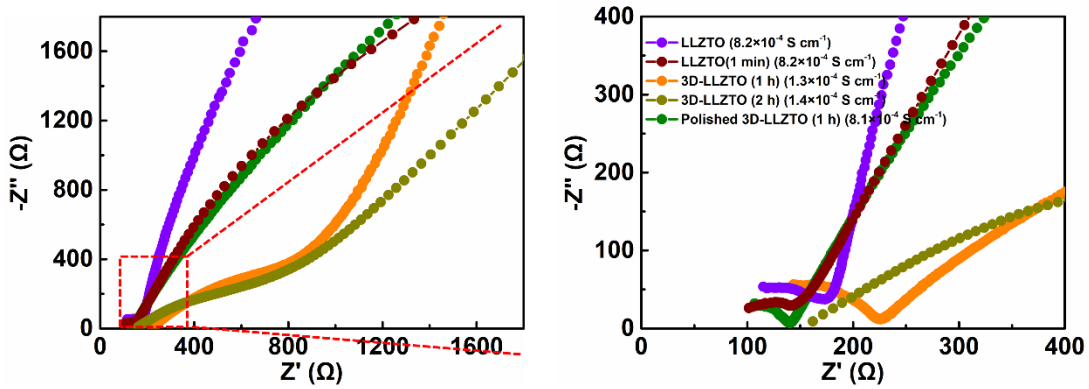

Figure S4 EIS spectra of LLZTO, LLZTO (1 min), 3D-LLZTO (1 h), 3D-LLZTO (2 h), and polished 3D-LLZTO (1 h).

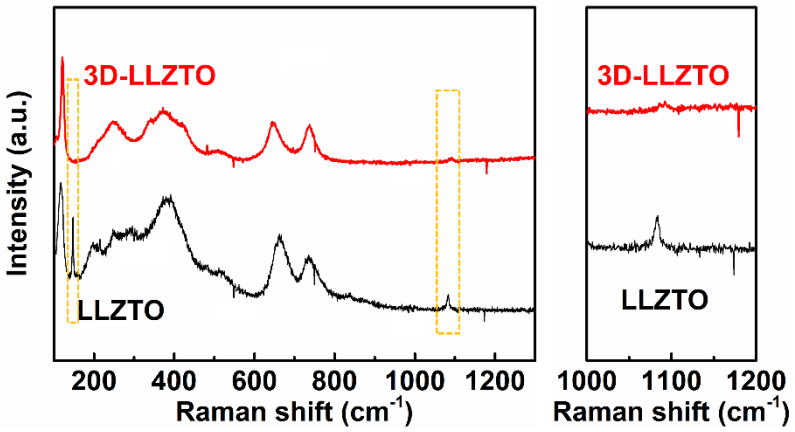

Figure S5 Raman spectra of the LLZTO and 3D-LLZTO by acid etching.

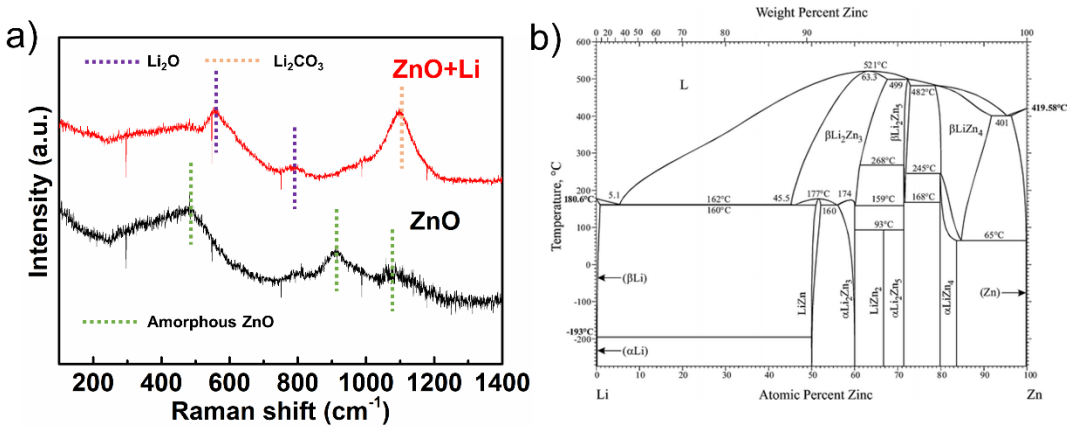

Figure S6 a) Raman spectra of the ZnO thin film on the glass plate and ZnO thin film contacted with molten Li on the glass plate. b) Zn-Li alloy phase diagram [3].

The interfacial contact can be greatly improved by the ZnO layer. We further characterized the reactions at the interface by Raman spectra. As shown in Fig. 4a, the peaks at 497, 908, and 1086 cm^{-1} correspond to the amorphous ZnO by ALD [4]. These peaks of ZnO disappear and the Li_2O peaks at 521 and 796 cm^{-1} are obtained when the ZnO is contacted with the molten Li at 300 °C. The enhanced wettability at the interface could be attributed to the conversion reaction between ZnO and Li (equation (1)).

$$ZnO\ (s) + Li\ (l) \rightarrow Li_2O\ (s) + Zn\ (s) \qquad (1)$$

Subsequently, the Zn further reacts with the Li to form alloy at 300 °C according to the Zn-Li alloy phase diagram (equation (2)). The as-formed Zn-Li alloy shows the excellent ion/electron conductivity, which can guide uniform Li deposition. It should be noted that the Li_2CO_3 peak at 1090 cm^{-1} could be attributed to the briefly exposed Li metal to air during the sample transfer for Raman testing.

$$Zn\ (s) + Li\ (l) \rightarrow LiZn\ (s) \qquad (2)$$

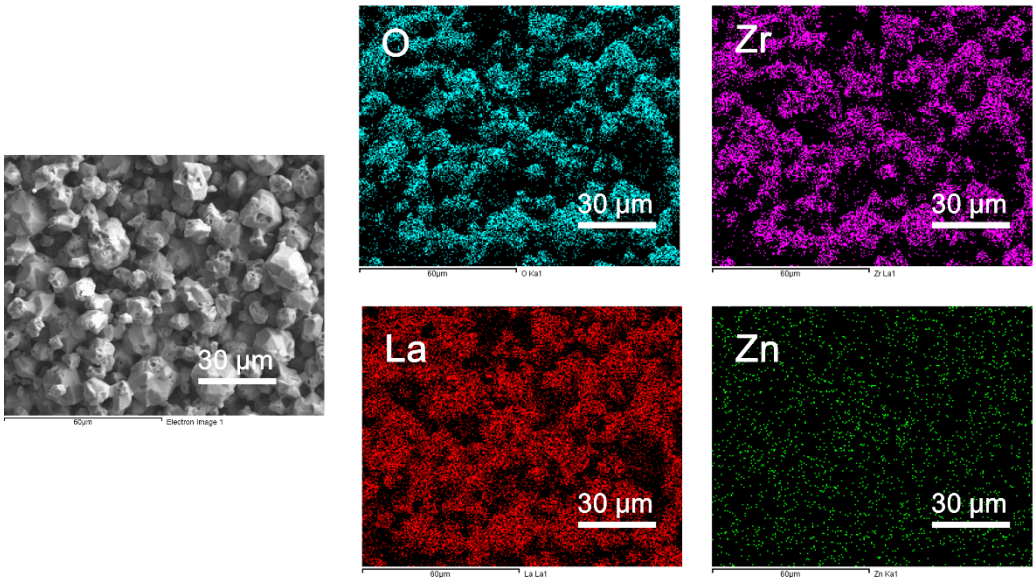

Figure S7 Top-view SEM images and EDS mappings of the 3D-LLZTO@ZnO pellet.

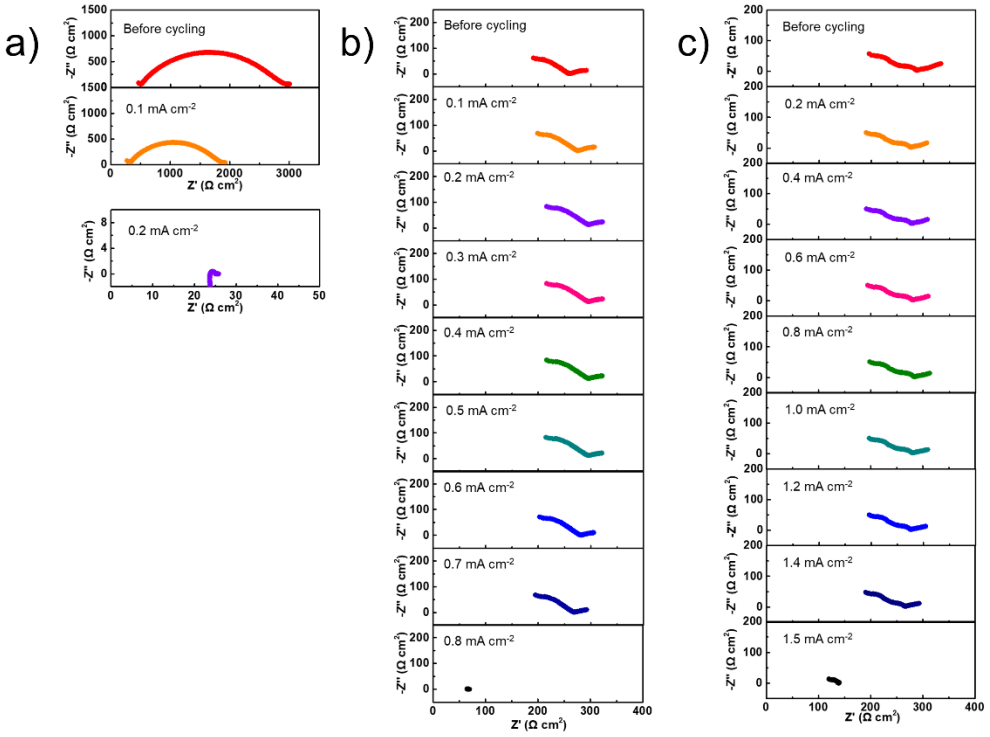

Figure S8 EIS spectra of a) Li/LLZTO/Li, b) Li/LLZTO@ZnO/Li, and c) Li/3D-LLZTO@ZnO/Li cells during CCD tests.

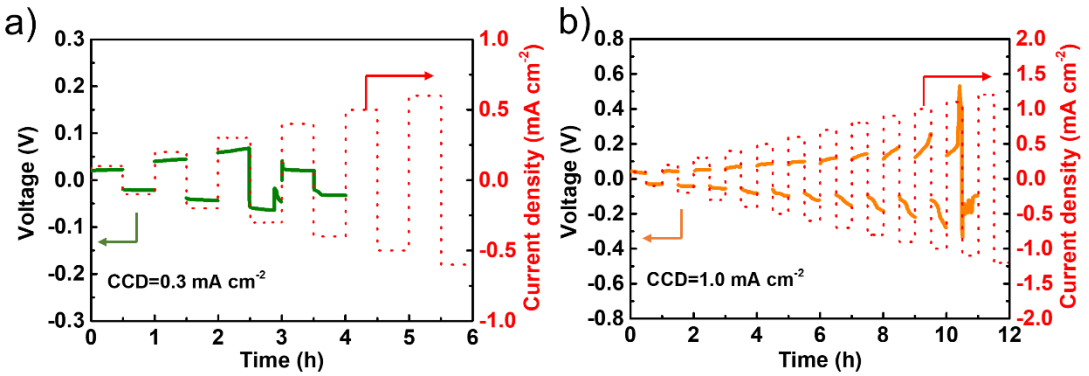

Figure S9 CCD of a) Li/LLZTO@ZnO/Li, and b) Li/3D-LLZTO@ZnO/Li cells with thin Li anodes (~30 μm).

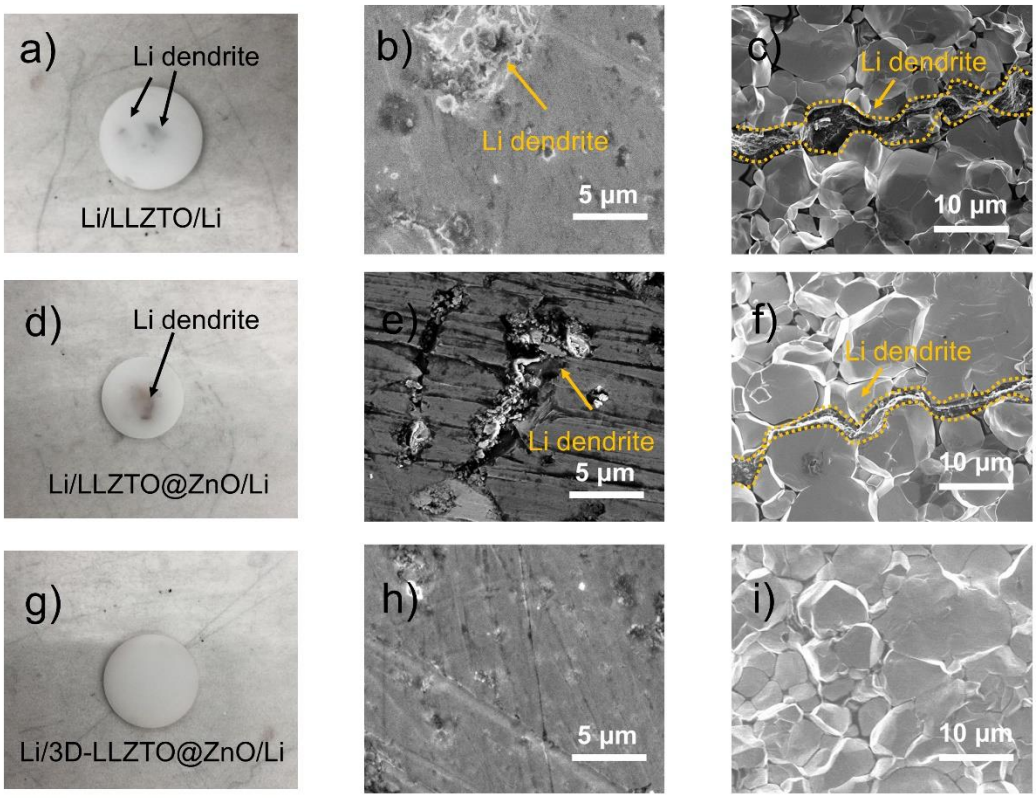

Figure S10 a) Optical image, b) surface morphology and c) cross-sectional SEM image of the Li/LLZTO/Li cell after short circuit at 0.5 cm^{-2} cycling. d) Optical image, e) surface morphology and f) cross-sectional SEM image of the Li/LLZTO@ZnO/Li cell after short circuit at 0.5 cm^{-2} cycling. g) Optical image, h) surface morphology and i) cross-sectional SEM image of the Li/3D-LLZTO@ZnO/Li cell after 600 h cycling at 0.5 cm^{-2} cycling. Note that the Li metal electrodes were removed by sanding.

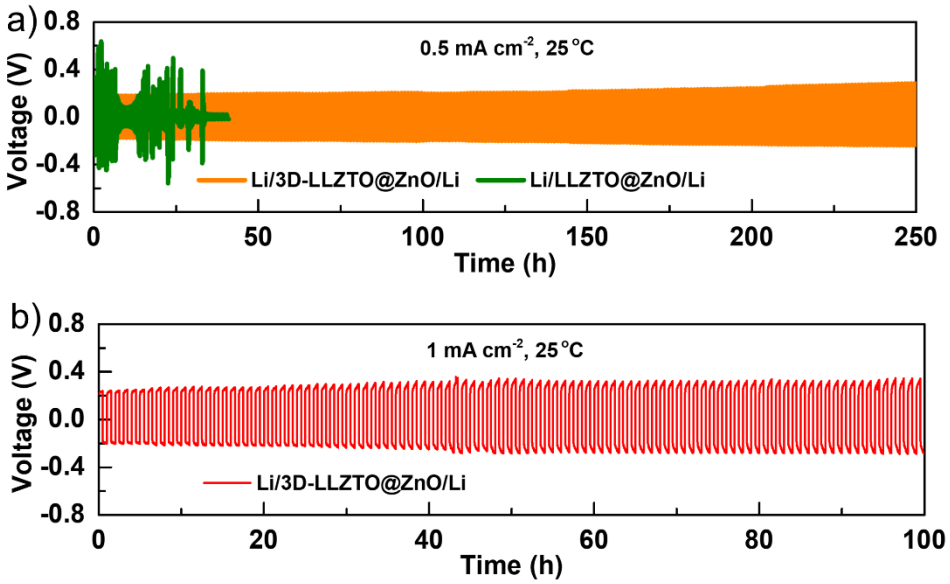

Figure S11 a) Galvanostatic cycling performance of the Li/LLZTO@ZnO/Li cell and Li/3D-LLZTO@ZnO/Li cell under 0.5 mA cm^{-2} (0.25 mAh cm^{-2}) at 25 °C. The thickness of Li anodes here is ~30 μm. b) Galvanostatic cycling performance of the Li/3D-LLZTO@ZnO/Li cell at 1 mA cm^{-2} (0.5 mAh cm^{-2}).

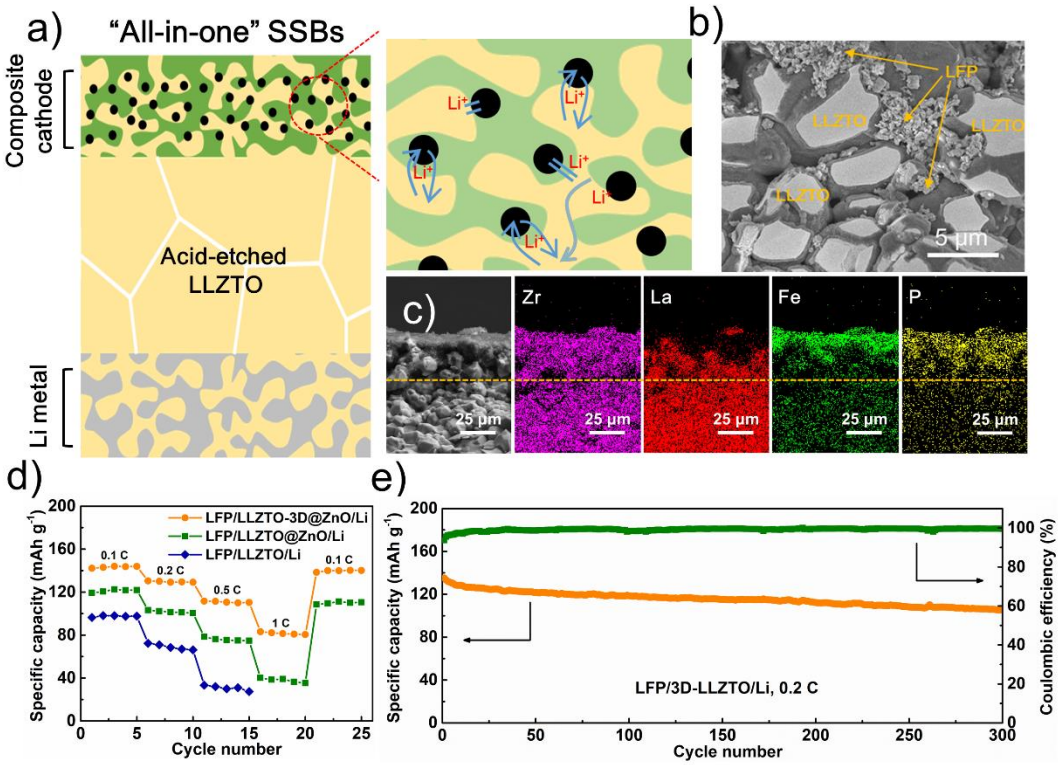

Figure S12 a) Schematic of "all-in-one" cells with a 3D Li anode and LFP cathode. b) cross-sectional SEM image and c) EDS mappings of the 3D LFP cathode. d) Rate performance of the LFP/LLZTO/Li, LFP/LLZTO@ZnO/Li and LFP/3D-LLZTO@ZnO/Li cells. e) Cycle performance of the LFP/3D-LLZTO@ZnO/Li cell under 0.2 C at 60 ºC.

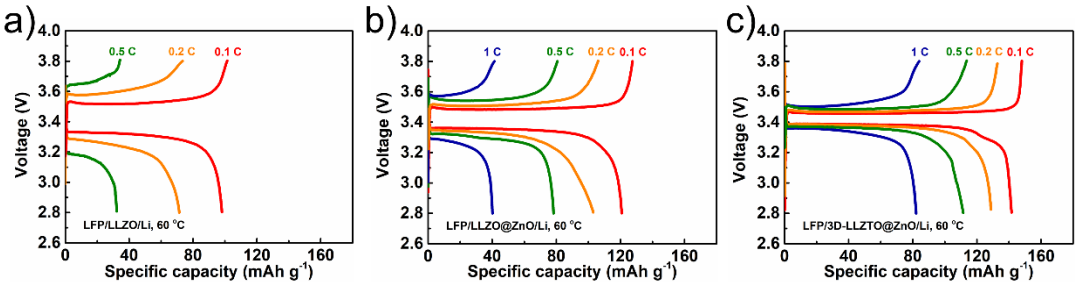

Figure S13 Charge/discharge curves of the LFP/LLZTO/LFP, LFP/LLZTO@ZnO/Li, and the LFP/3D-LLZTO@ZnO/Li cells at various current rates.

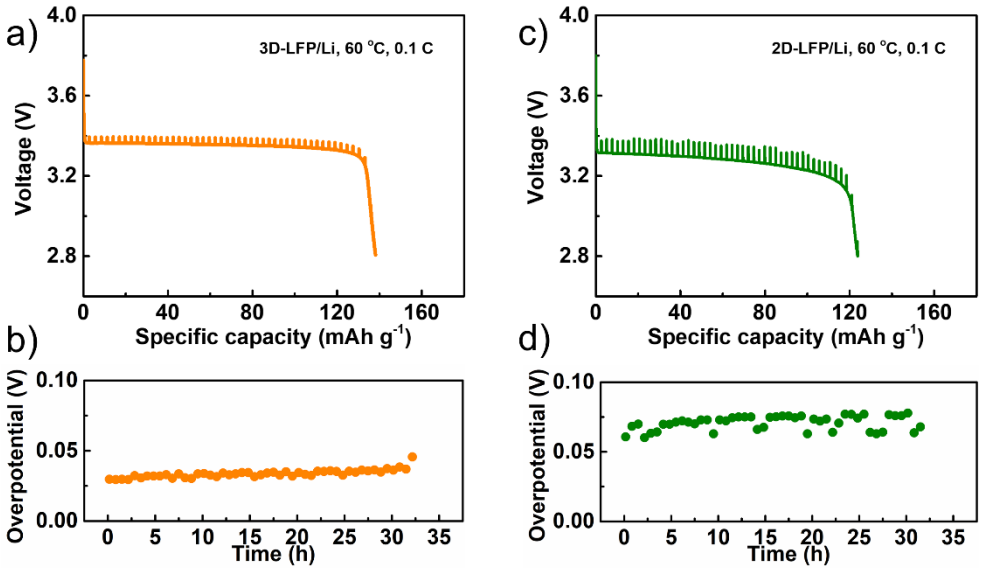

Figure S14 a) Transient discharge curves and b) polarization plots of 3D-LFP/Li cell under 0.1 C at 60 °C obtained by GITT. c) Transient discharge curves and d) polarization plots of 2D-LFP/Li cell under 0.1 C at 60 °C obtained by GITT.

References

(1) Du, F. M.; Zhao, N.; Li, Y. Q.; Chen, C.; Liu, Z. W.; Guo, X. X. All solid state lithium batteries based on lamellar garnet-type ceramic electrolytes. *J. Power Sources* **2015,** *300*, 24-28.

(2) Huo, H.; Zhao, N.; Sun, J.; Du, F.; Li, Y.; Guo, X. Composite electrolytes of polyethylene oxides/garnets interfacially wetted by ionic liquid for room-temperature solid-state lithium battery. *J. Power Sources* **2017,** *372*, 1-7.

(3) Pelton, A. The Li-Zn (lithium-zinc) system. *J.phase equilibria* **1991,** *12* (1), 42-45.

(4) Wang, Z.; Zhang, H.; Wang, Z.; Zhang, L.; Yuan, J.; Yan, S.; Wang, C. Structure and strong ultraviolet emission characteristics of amorphous ZnO films grown by electrophoretic deposition. *J. Mater. Res.* **2003,** *18* (1), 151-155.